A 2D Helmholtz equation solver library based on C++ and SuiteSparse

Rahul Sarkar and Biondo Biondi

ABSTRACT

We developed a 2D Helmholtz equation solver library in C++ based on the SuiteSparse library for sparse linear algebra. The solver library was successfully tested for correctness in this paper by running a suite of simple 2D examples. We first used the library to solve the Helmholtz equation in a homogenous medium for different frequency bands. The test was then repeated for an inhomogenous two layer medium, for the same frequency bands. We also performed Born linearization tests with the code and demonstrated that the error is quadratic in the magnitude of the velocity perturbation, in agreement with the theoretical prediction. Finally we performed extended linearized Born forward modeling tests using the Helmholtz code to demonstrate its use in Tomographic Full Waveform Inversion (TFWI) applications.

INTRODUCTION

Solving the wave equation in the frequency domain has many advantages from the perspective of seismic inversion. In particular, this is useful if we have a large number of shots, in which case the cost of pre-factoring and storing the LU decomposition of the matrix arising in the numerical solution of the Helmholtz equation is justified as it has to be performed only once for each frequency, and then the factors can be reused for all the shots. The solution to the Helmholtz equation is then obtained by performing a forward and backward solve for each shot. This idea also extends naturally to the TFWI setting introduced by Biondi and Almomin (2014), where one needs to solve the wave equation to get the background wave field which is then convolved with the extended model to get the secondary source to be propagated using Born modeling. In fact, one of the main motivations for this work is to be able to perform 3D TFWI at low frequencies below 5Hz, which can fit in present day computer memory for reasonably large model sizes. In addition to this, the convolution operation in time domain TFWI becomes a multiplication operation in the frequency domain. The same is also true of the gradient computation for certain objective functions such as in the case of FWI.

In this paper, we follow the discretization scheme introduced by Liu and Ying (2016). The code that we have developed can handle three kinds of boundary conditions: Dirichlet, Neumann and Sommerfeld radiation through a PML (perfectly matched

layer) approach as described in Liu and Ying (2016). The PML is implemented to have the same amount of attenuation across different frequency bands, and is also independent of the number of PML cells. We have implemented the Helmholtz solver in C++ using the SuiteSparse library (Davis, 2004, 2006) for performing the sparse factorization.

THEORY

In this section, we provide a very brief introduction to the Helmholtz equation, and outline the numerical scheme that we use to solve it in this paper. We establish the connection of the Helmholtz equation with the acoustic wave equation, derive formulas for the Born linearization of the Helmholtz equation, and also derive the frequency domain formulation of TFWI extended Born forward modeling.

The Helmholtz equation

The Helmholtz equation in d dimensions is given by

$$\left(\nabla^2 + \frac{\omega^2}{c^2(\mathbf{x})}\right)\hat{u}(\mathbf{x},\omega) = \hat{f}(\mathbf{x},\omega), \tag{1}$$

where $\mathbf{x} \in \mathbb{R}^d$, $\nabla^2 = \sum_{i=1}^{d} \frac{\partial^2}{\partial x_i^2}$ represents the d-dimensional Laplacian operator, $\omega \in \mathbb{R}$ is the angular frequency, $c(\mathbf{x})$ is the velocity of the medium that depends on the position $\mathbf{x}$, $\hat{f}(\mathbf{x},\omega)$ is the forcing function, and $\hat{u}(\mathbf{x},\omega)$ is the solution to the Helmholtz equation. For purposes of this paper, we will be only concerned with $d = 2$, i.e we will only consider the 2D Helmholtz equation.

Typically, the Helmholtz equation is solved on a bounded domain $\mathbf{\Gamma}$ with suitable boundary conditions on the boundary of the domain $\mathbf{d\Gamma}$, which forms a submanifold of $\mathbf{\Gamma}$ of codimension 1. Three types of boundary conditions are extremely common, namely *DBC(Dirichlet Boundary Condition)*, *NBC(Neumann Boundary Condition)* and *RBC(Robin Boundary Condition)*. These boundary conditions have the following analytical form

$$\begin{aligned}
\hat{u}(\mathbf{x},\omega)\Big|_{\mathbf{d\Gamma}} &= \hat{u}_D(\mathbf{x},\omega) \qquad (DBC) \\
\frac{\partial \hat{u}(\mathbf{x},\omega)}{\partial \mathbf{n}}\Big|_{\mathbf{d\Gamma}} &= \hat{u}_N(\mathbf{x},\omega) \qquad (NBC) \\
\left(a\hat{u}(\mathbf{x},\omega) + b\frac{\partial \hat{u}(\mathbf{x},\omega)}{\partial \mathbf{n}}\right)\Big|_{\mathbf{d\Gamma}} &= \hat{u}_R(\mathbf{x},\omega) \qquad (RBC),
\end{aligned} \tag{2}$$

where $\frac{\partial}{\partial \mathbf{n}}$ is the normal derivative operator pointing outward with respect to the boundary $\mathbf{d\Gamma}$.

However in many cases such as commonly encountered in frequency domain seismic inversion, one wishes to solve the Helmholtz equation on an unbounded domain. But even in such applications, the forcing function (also known as the "source") is still supported on a bounded domain, and one is interested in the solutions representing outgoing waves instead of the solutions representing incoming waves, i.e one wants the "source" to be a source and not a sink. To enforce this condition, a commonly used boundary condition is the Sommerfeld radiation boundary condition (see Sommerfeld (1949); Johnson (2008) for details), given by

$$\lim_{r\to\infty} \frac{\partial \hat{u}(\mathbf{x},\omega)}{\partial \mathbf{r}} - \frac{i\omega}{c_0}\hat{u}(\mathbf{x},\omega) = 0, \tag{3}$$

where we have assumed that the velocity of the medium is constant outside a bounded set $\mathbf{\Gamma}$, i.e $c(\mathbf{x})\Big|_{\mathbb{R}^d\setminus\mathbf{\Gamma}} = c_0$, and $\frac{\partial}{\partial \mathbf{r}}$ denotes the derivative operator along the unit normal in the radial direction. In practice, one has to solve the Helmholtz equation on a truncated domain in a computer, where the Sommerfeld radiation boundary condition is implemented using some form of PML condition, which we discuss next.

Numerical scheme to solve the Helmholtz equation

The numerical scheme implemented for this paper is taken from Liu and Ying (2016). Both directions are treated in a manner similar to one another, and thus we only discuss what is done along the X direction. Suppose our computational domain along the X direction is given by $[0, l]$. Let η denote the PML width, and let us first discuss the case when we have PML boundaries on both ends of the computational domain. Thus we have two PML zones given by $[0, \eta)$ and $(l-\eta, l]$. Following Liu and Ying (2016), we introduce the auxiliary functions

$$\begin{aligned}
\sigma(x) &:= \begin{cases} \frac{C}{\eta}\left(\frac{x-\eta}{\eta}\right)^2, & x \in [0,\eta), \\ 0, & x \in [\eta, l-\eta], \\ \frac{C}{\eta}\left(\frac{x-l+\eta}{\eta}\right)^2, & x \in (l-\eta, l], \end{cases} \\
s(x) &:= \left(1 + i\frac{\sigma(x)}{\omega}\right)^{-1},
\end{aligned} \tag{4}$$

where C is a positive constant that does not depend on ω, and η is typically around one wavelength.

With this notation, the Helmholtz equation along X direction with PML is modified to be

$$\begin{aligned}
&\left(\left(s(x)\frac{\partial}{\partial x}\right)^2 + \frac{\omega^2}{c^2(x)}\right)\hat{u}(x,\omega) = \hat{f}(x,\omega), \quad \forall\, x \in [0,l], \\
&\text{with } \hat{u}(0,\omega) = \hat{u}(l,\omega) = 0, \text{ and } \hat{f}(x,\omega) = 0 \text{ in the PML zone.}
\end{aligned} \tag{5}$$

The above equation 5 is discretized using a standard second-order central difference numerical scheme as follows

$$\frac{s_i}{h_x}\left(\frac{s_{i+1/2}}{h_x}(\hat{u}_{i+1}-\hat{u}_i)-\frac{s_{i-1/2}}{h_x}(\hat{u}_i-\hat{u}_{i-1})\right)+\frac{\omega^2}{c_i^2}\hat{u}_i=\hat{f}_i,\ \ \forall\, 1\le i\le n, \qquad (6)$$

where the subscript i means that the corresponding quantity is evaluated at $x = ih_x$, and $h_x = \frac{1}{n+1}$ is the grid size along X. Note that here we have used the same PML width on both sides, but it is possible to use different PML widths also, as long as they are kept to at least one wavelength. Then the discretization scheme gets modified accordingly. Finally one should also note that it is possible to discretize equation 5 using a higher order discretization scheme which is relatively straightforward to perform, but we do not explore this in our paper.

When one has DBC on any side, we set $\eta = 0$ for that side. The case of NBC is similar, and we first set $\eta = 0$ for that side followed by using a central difference scheme for the points on the boundary. The right hand sides are also modified by the DBC and NBC, depending on the numerical values supplied for the boundary conditions.

Performing the above discretization leads to a matrix equation of the form $\mathbf{A}\hat{\mathbf{u}} = \hat{\mathbf{f}}$. The matrix $\mathbf{A}$ is extremely sparse and has at most 5 non-zero elements per row in the case of the 2D Helmholtz equation. We use SuiteSparse to compute the sparse LU factorization of such a system and then one can solve the same equation for different right hand sides, such as for different shots.

Connection of the Helmholtz equation with the wave equation

To understand how the Helmholtz equation arises in frequency domain seismic inverse problems, let us consider the constant density acoustic wave equation in a medium with heterogenous velocities given by

$$\frac{1}{c^2(\mathbf{x})}\frac{\partial^2 u(\mathbf{x},t)}{\partial t^2}-\nabla^2 u(\mathbf{x},t)=-f(\mathbf{x},t), \qquad (7)$$

where $u(\mathbf{x}, t)$ is the solution to the wave equation, $-f(\mathbf{x}, t)$ is the time domain forcing function (also called the "source") and $c(\mathbf{x})$ denotes the heterogenous velocity field as defined earlier.

To see the connection with the Helmholtz equation, we simply Fourier transform equation 7 in time and we obtain the Helmholtz equation in equation 1, where $\hat{u}(\mathbf{x}, \omega)$ and $\hat{f}(\mathbf{x}, \omega)$ are the Fourier transforms of $u(\mathbf{x}, t)$ and $f(\mathbf{x}, t)$ respectively. Thus the solution to the time domain wave equation is completely determined if we know the solution to the corresponding Helmholtz equation for all $\omega \in \mathbb{R}$, by Fourier duality. In practice, the source $f(\mathbf{x}, t)$ is band limited and thus one only needs to solve the Helmholtz equation for a limited range of frequencies.

Linearization of the Helmholtz equation

We next derive formulas for the Born linearization of the Helmholtz equation, for a fixed angular frequency ω. Let us consider the velocity field $c(\mathbf{x})$ and the corresponding solution to the Helmholtz equation $\hat{u}(\mathbf{x},\omega)$ appearing in equation 1. We now perturb the velocity field by adding a small perturbation $\delta c(\mathbf{x})$, and so the new velocity is given by $c(\mathbf{x}) + \delta c(\mathbf{x})$. As a result of this perturbation, the solution to the Helmholtz equation also changes and let us denote it by $\hat{u}(\mathbf{x},\omega) + \delta\hat{u}(\mathbf{x},\omega)$. These perturbed quantities also satisfy the Helmholtz equation, and so we have

$$\left(\nabla^2 + \frac{\omega^2}{(c(\mathbf{x}) + \delta c(\mathbf{x}))^2}\right)(\hat{u}(\mathbf{x},\omega) + \delta\hat{u}(\mathbf{x},\omega)) = \hat{f}(\mathbf{x},\omega). \tag{8}$$

The Born linearization formula expresses the first order relationship between the perturbed quantities $\delta\hat{u}(\mathbf{x},\omega)$ and $\delta c(\mathbf{x})$. To achieve this goal, we first note that to first order we have the following result

$$\frac{\omega^2}{(c(\mathbf{x}) + \delta c(\mathbf{x}))^2} \approx \frac{\omega^2}{c^2(\mathbf{x})}\left(1 - 2\frac{\delta c(\mathbf{x})}{c(\mathbf{x})}\right). \tag{9}$$

Then using equation 9, and subtracting equation 1 from equation 8 and retaining only the first order terms we get

$$\left(\nabla^2 + \frac{\omega^2}{c^2(\mathbf{x})}\right)\delta\hat{u}(\mathbf{x},\omega) = 2\omega^2\frac{\delta c(\mathbf{x})}{c^3(\mathbf{x})}\hat{u}(\mathbf{x},\omega). \tag{10}$$

The above equation 10 is the linearized Born formula for the Helmholtz equation.

TFWI extended linearized Born forward modeling

A great advantage of solving the wave equation in the frequency domain is that TFWI extended Born linearized forward modeling also becomes straightforward. We first recall the time domain wave equation for the same as formulated in Biondi and Almomin (2014),

$$\frac{1}{c^2(\mathbf{x})}\frac{\partial^2 u_e(\mathbf{x},t)}{\partial t^2} - \nabla^2 u_e(\mathbf{x},t) = \int_{\mathbb{R}} 2\frac{\partial^2 u}{\partial t^2}(\mathbf{x},t-\tau)\frac{\delta c_e(\mathbf{x},\tau)}{c^3(\mathbf{x})}\,d\tau, \tag{11}$$

where $u(\mathbf{x},t)$ solves equation 7, $\delta c_e(\mathbf{x},t)$ is the extended velocity model, and $u_e(\mathbf{x},t)$ is the extended Born linearized forward modeled data.

We can Fourier transform equation 11 with respect to time to get the corresponding Helmholtz equation in the frequency domain given by

$$\left(\nabla^2 + \frac{\omega^2}{c^2(\mathbf{x})}\right)\hat{u}_e(\mathbf{x},\omega) = \frac{2\omega^2}{c^3(\mathbf{x})}\hat{u}(\mathbf{x},\omega)\delta\hat{c}_e(\mathbf{x},\omega), \tag{12}$$

where $\hat{u}_e(\mathbf{x}, \omega)$ is the Fourier transform of $u_e(\mathbf{x}, t)$, and $\delta\hat{c}_e(\mathbf{x}, \omega)$ is the Fourier transform of $\delta c_e(\mathbf{x}, t)$. As can be seen from equation 12, in order to compute $\hat{u}_e(\mathbf{x}, \omega)$, we only need to change the forcing term in the Helmholtz equation and moreover the forcing term is just a point wise multiplication for each frequency ω. Thus, we have been able to reduce the expensive convolution operation in time domain to a trivial multiplication operation, while at the same time the Helmholtz operator on the left remains unchanged which means that the matrix factorization can be reused.

NUMERICAL EXPERIMENTS

In this section, we present some numerical tests in 2D performed with the 2D Helmholtz equation solver library. For the first four tests, our simulation geometry consists of 500×500 cells along X and Z directions. The top left corner of the geometry has the coordinates $(0 \text{ km}, 0 \text{ km})$. The simulation box dimensions along the two directions are 10 km $\times$ 10 km, which gives a grid spacing of 0.02 km along both the X and Z directions. In the first and second tests we solve the Helmholtz equation in a homogenous medium and a heterogenous two layer medium, respectively. In the third numerical experiment, we test the accuracy of the Born linearization, while in the fourth experiment we test the free-surface boundary condition for the top surface which is encountered for example while dealing with the air-water interface. For the fifth and final test, we perform extended linearized Born forward modeling in a homogenous background medium with the extended model given by a point scatterer. In all the cases, we plot both the real and imaginary parts of the solution to the Helmholtz equation.

Homogenous velocity field

In this experiment, we use a constant homogenous velocity $c(\mathbf{x}) = 1$ km/s. We place the source at the center of the model at $(5 \text{ km}, 5 \text{ km})$. We use PML boundary conditions on all sides of the model. We show the results for two different values of angular frequency — Figures 1a and 1b show the results for $\omega = 20$ rad/sec, and Figures 2a and 2b show the results for $\omega = 40$ rad/sec. Visual inspection of the figures reveal agreement with what we expect of the solutions - the wavelength of the solution for $\omega = 20$ rad/sec is twice that of the wavelength of the solution for $\omega = 40$ rad/sec. Moreover, we see that the solutions are spherically symmetric which is what we expect.

Heterogenous velocity field

In this experiment, we use a heterogenous two-layer velocity model that is constant horizontally, given by $c(\mathbf{x}) = 1$ km/s for $z =$ 0-5 km, and $c(\mathbf{x}) = 2$ km/s for $z =$ 5-10 km. We place the source at the coordinates $(5 \text{ km}, 2.5 \text{ km})$. We again use

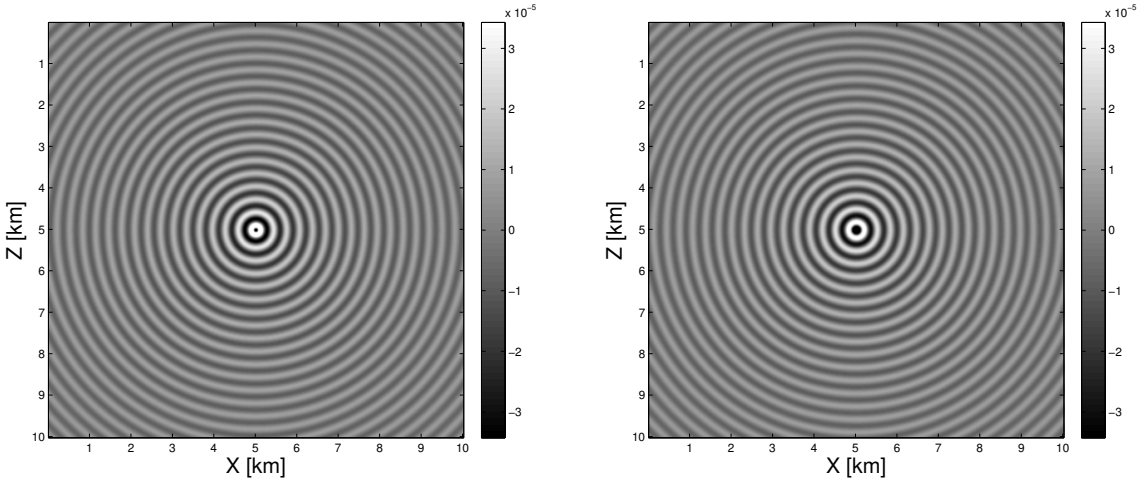

(a) (b)

Figure 1: Solution to the Helmholtz equation with a constant velocity medium $c(\mathbf{x}) =$ 1 km/s, for $\omega = 20$ rad/sec, and a unit impulse source placed at (5 km, 5 km) : a) Real part, b) Imaginary part. [**ER**]

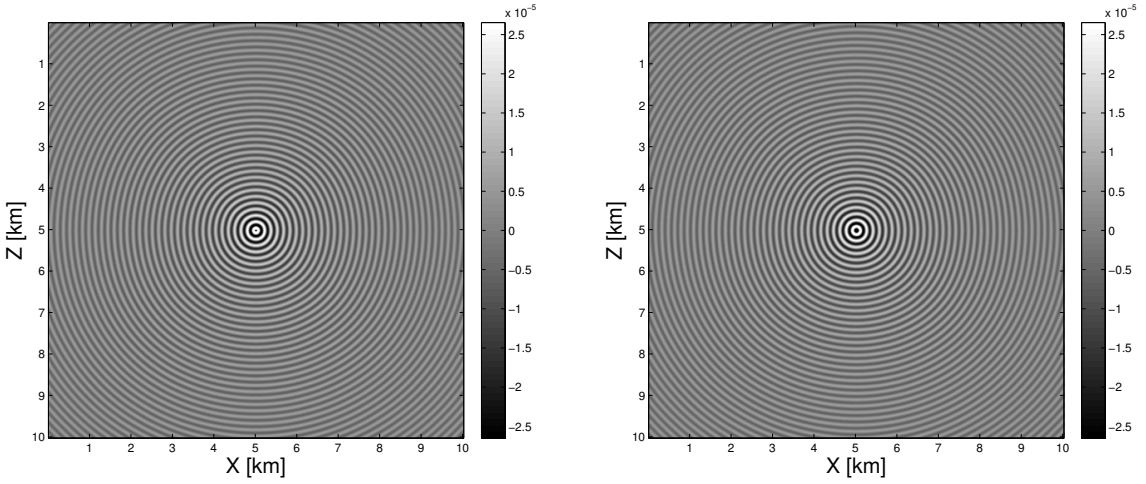

(a) (b)

Figure 2: Solution to the Helmholtz equation with a constant velocity medium $c(\mathbf{x}) =$ 1 km/s, for $\omega = 40$ rad/sec, and a unit impulse source placed at (5 km, 5 km) : a) Real part, b) Imaginary part. [**ER**]

PML boundary conditions on all sides of the model and show the results for two different values of angular frequency — Figures 3a and 3b show the results for $\omega = 20$ rad/sec, and Figures 4a and 4b show the results for $\omega = 40$ rad/sec. The figures reveal superposition between direct waves from the source and reflected waves from the interface in the top layer, while we only have transmitted waves in the bottom layer. Also the wavelength of the solution is twice in the second layer as compared to the first layer, which is expected theoretically.

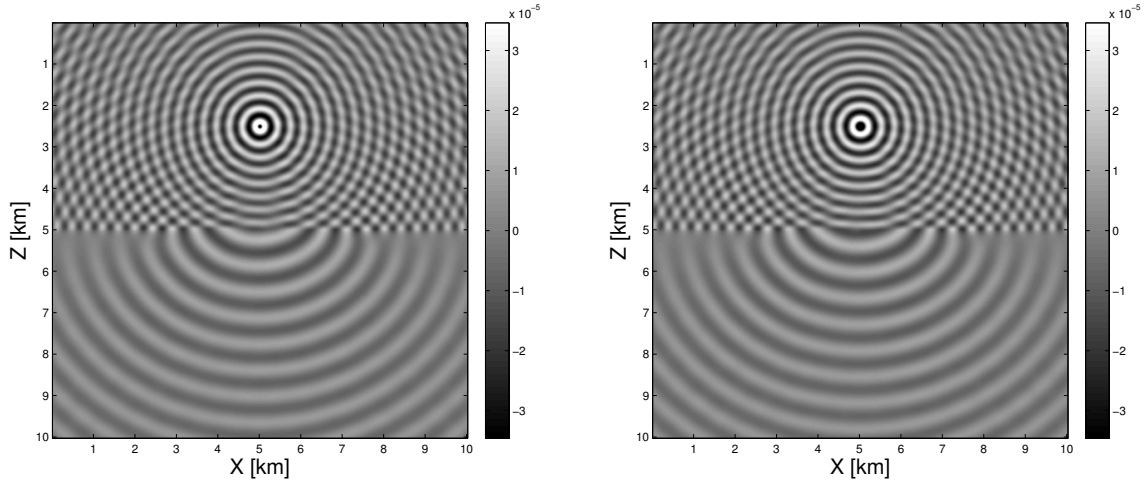

(a) (b)

Figure 3: Solution to the Helmholtz equation at $\omega = 20$ rad/sec with a two layer (horizontally constant) medium given by $c(\mathbf{x}) = 1$ km/s for $z = 0$-5 km, and $c(\mathbf{x}) = 2$ km/s for $z = 5$-10 km, and a unit impulse source placed at $(5 \text{ km}, 2.5 \text{ km})$: a) Real part, b) Imaginary part. [**ER**]

Linearized Born scattering

In the linearized Born scattering tests, we design the experiment using a constant velocity background medium given by $c(\mathbf{x}) = 1$ km/s with the source placed at the center of the model at $(5 \text{ km}, 5 \text{ km})$. The Helmholtz equation is solved to obtain the background solution $\hat{u}(\mathbf{x}, \omega)$. We use PML boundary conditions on all sides of this model for this test, and set the angular frequency $\omega = 20$ rad/sec. Next, we create a velocity perturbation at a single point in the model at $(5 \text{ km}, 7.5 \text{ km})$ of 10% (0.1 km/s), and zero everywhere else. This is our $\delta c(\mathbf{x})$.

We first create a new velocity model by adding the perturbation to the background velocity, given by $\widetilde{c}(\mathbf{x}) = c(\mathbf{x}) + \delta c(\mathbf{x})$. The Helmholtz equation is then solved to get the new solution given by $\widehat{\widetilde{u}}(\mathbf{x}, \omega)$. We then calculate the true perturbed solution as $\widetilde{\delta \hat{u}}(\mathbf{x}, \omega) = \widehat{\widetilde{u}}(\mathbf{x}, \omega) - \hat{u}(\mathbf{x}, \omega)$. The real and imaginary components of the true perturbed wave field generated this way are plotted in Figures 5a and 5b respectively.

Next, we perform linearized Born modeling using equation 10 to get a first order

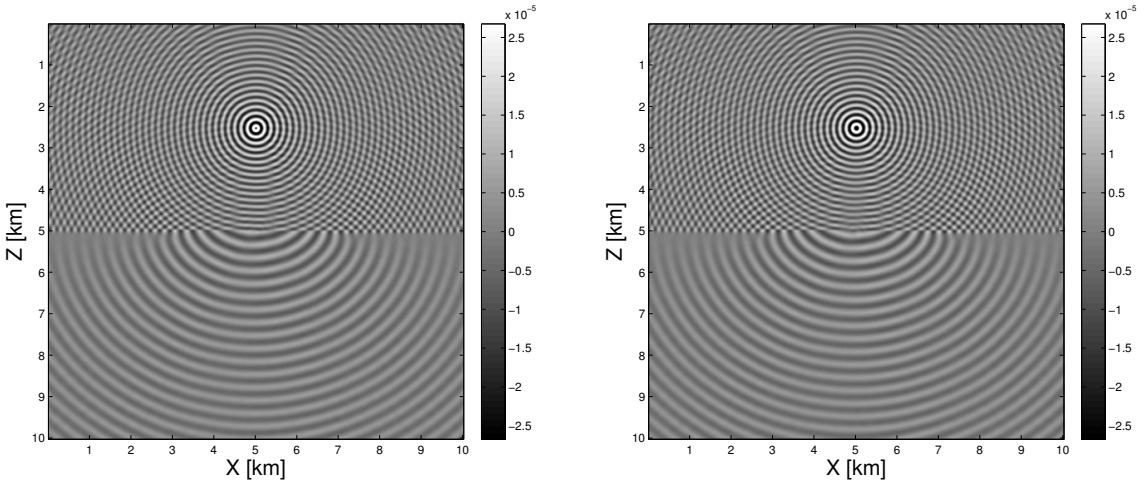

(a) (b)

Figure 4: Solution to the Helmholtz equation at $\omega = 40$ rad/sec with a two layer (horizontally constant) medium given by $c(\mathbf{x}) = 1$ km/s for $z = 0$-5 km, and $c(\mathbf{x}) = 2$ km/s for $z = 5$-10 km, and a unit impulse source placed at $(5 \text{ km}, 2.5 \text{ km})$: a) Real part, b) Imaginary part. [**ER**]

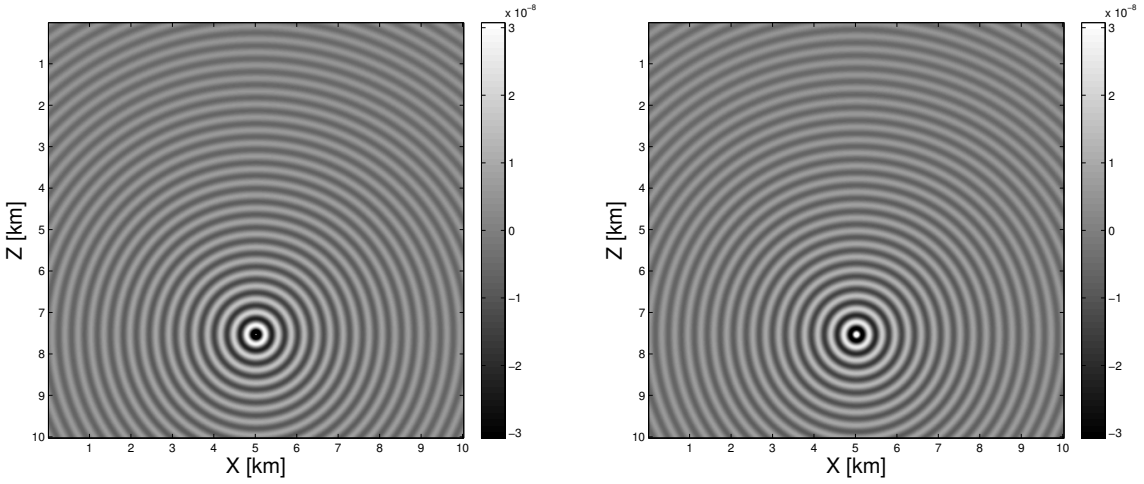

(a) (b)

Figure 5: True difference between the solutions to the Helmholtz equation $\hat{u}(\mathbf{x}, \omega)$ and $\widetilde{\hat{u}}(\mathbf{x}, \omega)$ at $\omega = 20$ rad/sec, formed respectively using a constant velocity background medium given by $c(\mathbf{x}) = 1$ km/s, and that with a perturbed medium obtained by adding 0.1 km/s to the background at $(5 \text{ km}, 7.5 \text{ km})$. The primary source is a unit impulse located at $(5 \text{ km}, 5 \text{ km})$. The quantity plotted is the perturbed wave field $\widetilde{\delta\hat{u}}(\mathbf{x}, \omega) = \widetilde{\hat{u}}(\mathbf{x}, \omega) - \hat{u}(\mathbf{x}, \omega)$: a) Real part, b) Imaginary part. [**ER**]

estimate of the true perturbed solution, given by $\delta\hat{u}(\mathbf{x},\omega)$. The real and imaginary components of $\delta\hat{u}(\mathbf{x},\omega)$ are plotted in Figures 6a and 6b respectively. As we can see from the colorbars, the amplitudes of $\widetilde{\delta\hat{u}}(\mathbf{x},\omega)$ are much lower compared to $\delta\hat{u}(\mathbf{x},\omega)$. However, the solutions resemble each other upon visual inspection. The errors can be attributed to the relatively large magnitude of the velocity perturbation, which is expected to decrease as we reduce the magnitude of the perturbation at a quadratic rate. This is what we demonstrate next.

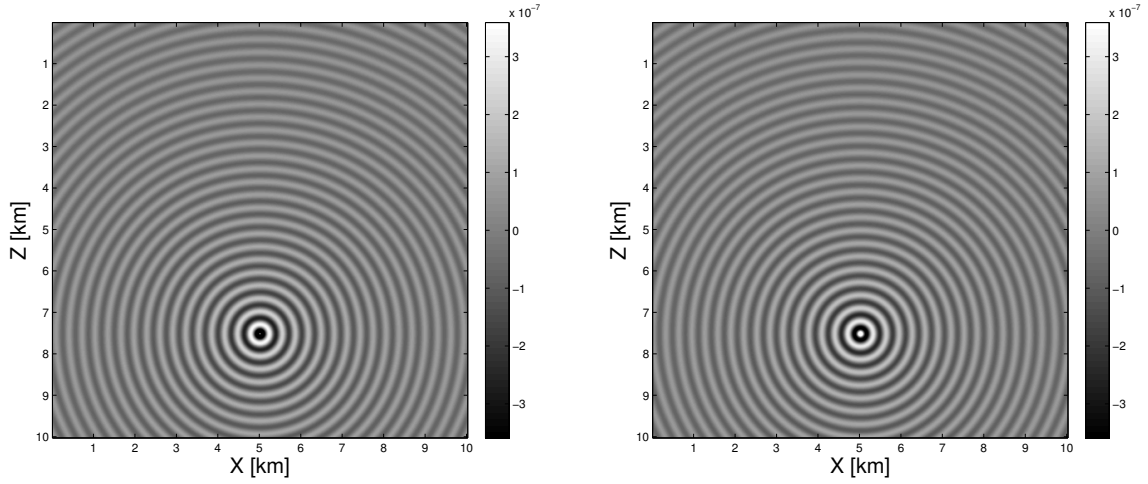

(a) (b)

Figure 6: First order estimate of the perturbed wave field using Born modeling $\widetilde{\delta\hat{u}}(\mathbf{x},\omega)$ at $\omega = 20$ rad/sec, with a scatterer located at (5 km, 7.5 km) of 0.1 km/s : a) Real part, b) Imaginary part. [**ER**]

We proceed by varying the velocity perturbation $\delta c(\mathbf{x})$ placed at the same location as before, but this time varying it from 1%, 2%,...,10%. The quantities $\widetilde{\delta\hat{u}}(\mathbf{x},\omega)$ and $\delta\hat{u}(\mathbf{x},\omega)$ are recalculated for each case and then we calculate the 2-norm of the difference $||\widetilde{\delta\hat{u}}(\mathbf{x},\omega) - \delta\hat{u}(\mathbf{x},\omega)||_2$. The results are plotted in Figure 7. As we can see from the image, the relationship is approximately quadratic.

Free surface modeling

In this experiment, we use a constant homogenous velocity $c(\mathbf{x}) = 1$ km/s, and place the source at the center of the model at (5 km, 5 km), just like the first numerical experiment. We use PML boundary conditions on the left, right and bottom sides of the model. But to simulate the air-water interface on the top of the model, we use the homogenous Neumann boundary condition on the top side. This is expected to generate reflections from the top surface. We show the results for two different values of angular frequency — Figures 8a and 8b show the results for $\omega = 20$ rad/sec, and Figures 9a and 9b show the results for $\omega = 40$ rad/sec.

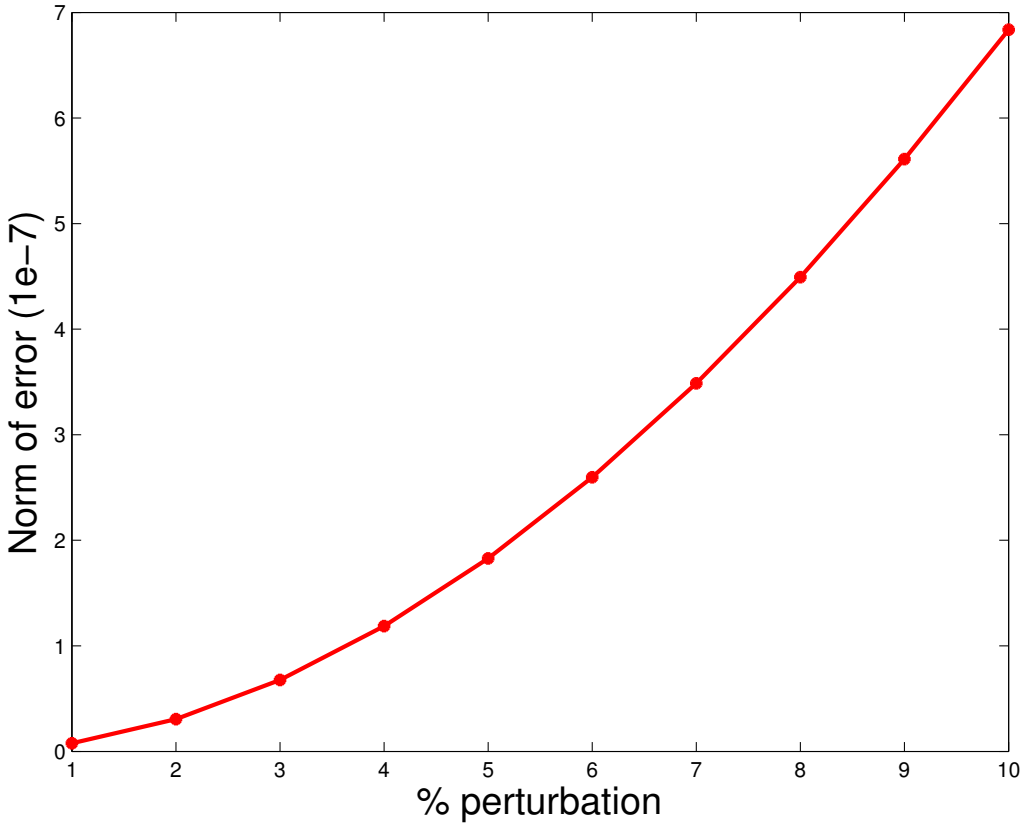

Figure 7: Plot of the norm of the error $||\widetilde{\delta\hat{u}}(\mathbf{x},\omega)-\delta\hat{u}(\mathbf{x},\omega)||_2$ vs $\frac{\delta c(\mathbf{x})}{c(\mathbf{x})}\%$, where $\widetilde{\delta\hat{u}}(\mathbf{x},\omega)$ is the first order Born scattered wave field and $\delta\hat{u}(\mathbf{x},\omega)$ is the true perturbed wave field. [**CR**]

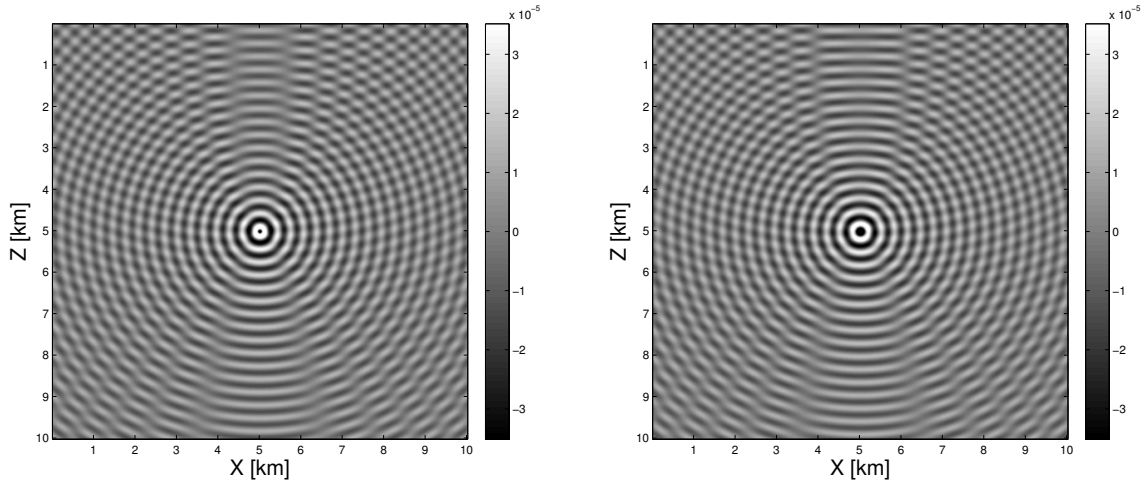

(a) (b)

Figure 8: Solution to the Helmholtz equation with a constant velocity medium $c(\mathbf{x}) = 1$ km/s, for $\omega = 20$ rad/sec, and a unit impulse source placed at $(5\text{ km}, 5\text{ km})$, and homogenous Neumann Boundary Conditions on the top side : a) Real part, b) Imaginary part. [**ER**]

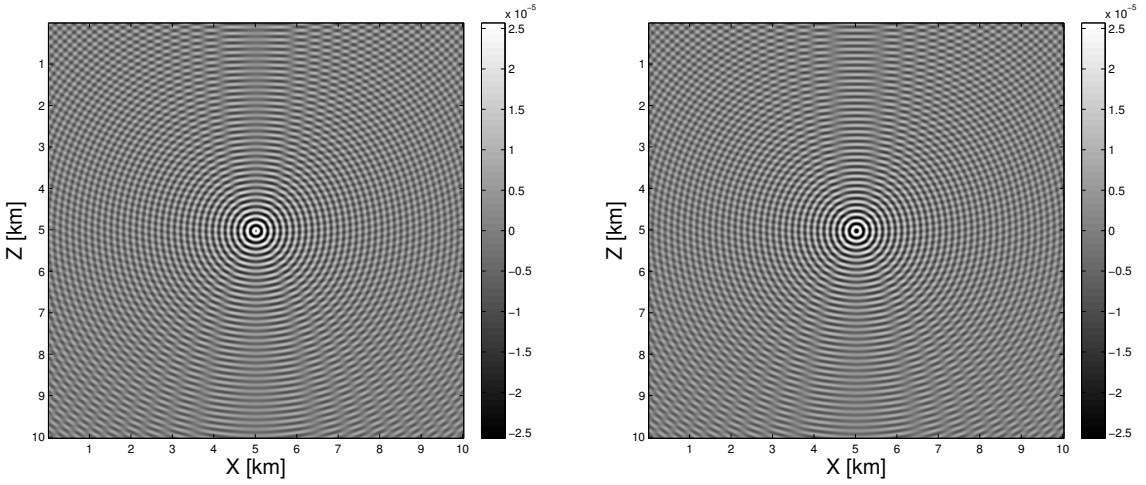

(a) (b)

Figure 9: Solution to the Helmholtz equation with a constant velocity medium $c(\mathbf{x}) = 1$ km/s, for $\omega = 40$ rad/sec, and a unit impulse source placed at (5 km, 5 km), and homogenous Neumann Boundary Conditions on the top side : a) Real part, b) Imaginary part. [**ER**]

TFWI forward modeling

The goal of the last and final experiment is to perform TFWI linearized extended Born forward modeling using the Helmholtz equation, as described in equation 12. We will also attempt to reconstruct the time domain recorded waveform in this experiment. We start by using a constant homogenous velocity medium with $c(\mathbf{x}) = 5$ km/s as the background, and place the source at the center of the model. However this time instead of using a point source, we choose a spatially varying Gaussian source (in both X and Z directions) centered at ($x_0 = 5$ km, $z_0 = 5$ km) and standard deviation $\sigma = 0.1$ km, with the source injected in phase at all the spatial points. Thus, if we denote the time domain wavelet as $w(t)$, then the time domain source denoted by $f(\mathbf{x}, t)$ is given as

$$f(\mathbf{x}, t) = w(t) \frac{1}{\sqrt{2\pi\sigma^2}} \exp\left(-\frac{(x - x_0)^2 + (z - z_0)^2}{2\sigma^2}\right). \tag{13}$$

We use a Ricker wavelet $w(t)$ with peak frequency $f_p = 10$ Hz, sampling interval $\Delta t = 8$ ms, number of samples $N_t = 250$ and a delay of $\delta t = 0.2$ s. This gives us a total modeling time of $N_t \Delta t = 2$ s. The functional form of the wavelet is given by

$$w(t) = (1 - 2\pi^2 f_p^2 (t - \delta t)^2) \exp\left(-\pi^2 f_p^2 (t - \delta t)^2\right). \tag{14}$$

The wavelet $w(t)$ and its amplitude spectrum are plotted in Figures 10a and 10b respectively, while the spatially varying Gaussian field for source injection is shown in Figure 10c.

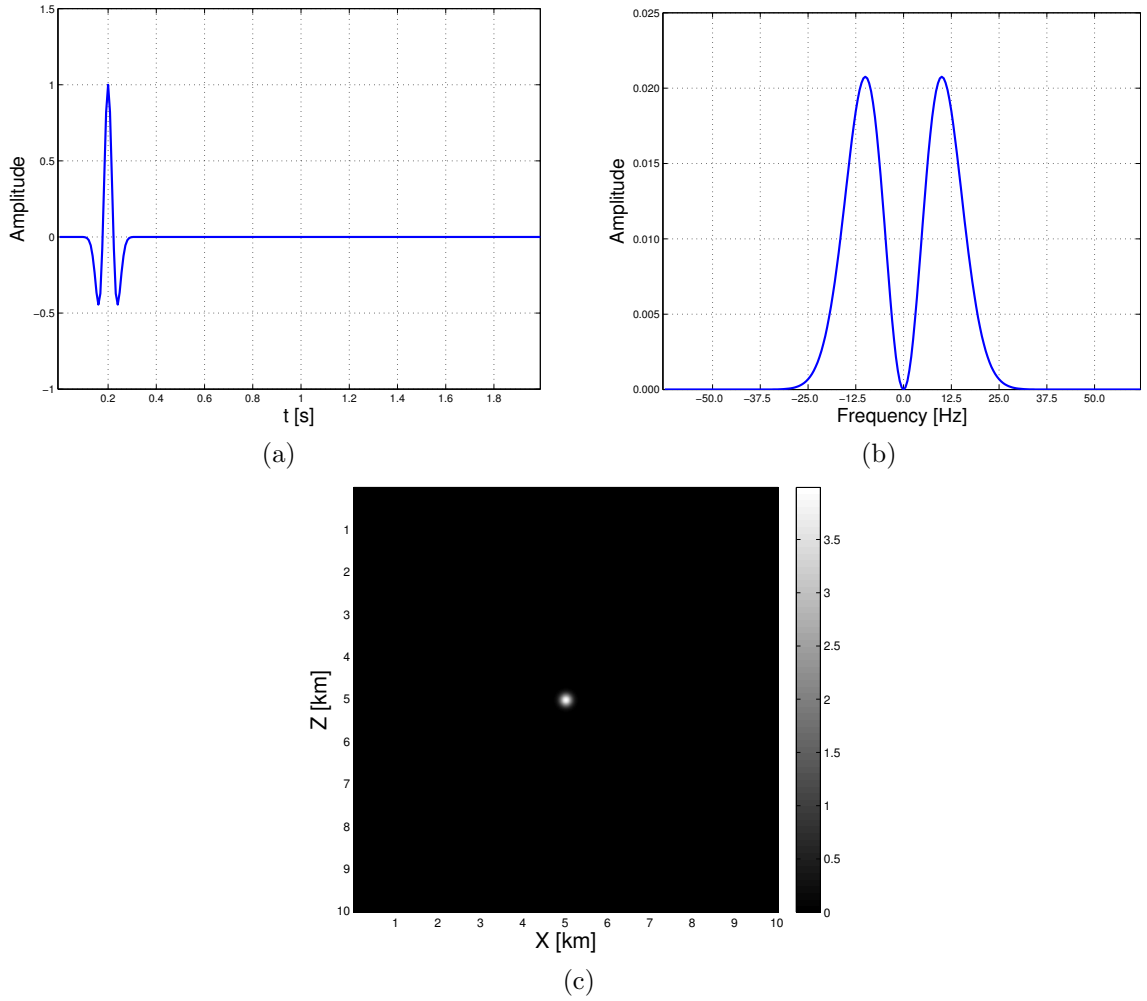

Figure 10: Source function $f(\mathbf{x}, t)$ used for the TFWI experiment : a) Ricker wavelet in time $w(t)$, b) Amplitude spectra of $w(t)$, c) Spatially varying Gaussian field used for source injection. [**CR**]

The source function $f(\mathbf{x}, t)$ is then discrete Fourier transformed in time, which gives us an angular frequency sampling of $\Delta\omega = \frac{2\pi}{N_t \Delta t}$. The Fourier transformed coefficients of $f(\mathbf{x}, t)$ correspond to the N_t angular frequencies given by the ordered set $\left\{\left(-\frac{N_t}{2}+1\right)\Delta\omega, \ldots, 0, \ldots, \frac{N_t}{2}\Delta\omega\right\}$, where the angular frequencies are spaced by units of $\Delta\omega$. This gives us the set of frequencies for which we need to solve the Helmholtz equation. However, because the time domain solution to the wave equation is purely real, the solution to the Helmholtz equation satisfies the following symmetry condition

$$\hat{u}(\mathbf{x}, -\omega) = \hat{u}(\mathbf{x}, \omega)^*, \tag{15}$$

which means that we only need to solve the Helmholtz equation for the positive frequencies, and the solutions for the negative frequencies are obtained simply by complex conjugation. Once all the solutions for the different frequencies have been found by solving the Helmholtz equation, we can inverse discrete Fourier transform the solution to get the time domain wave field.

In order to demonstrate this process, we place our receivers at a depth given by $z = 2.5$ km, and for all grid points in the X direction. We first solve for the background wave field using this process and the resulting time domain wave field at the receiver locations is shown in Figure 11.

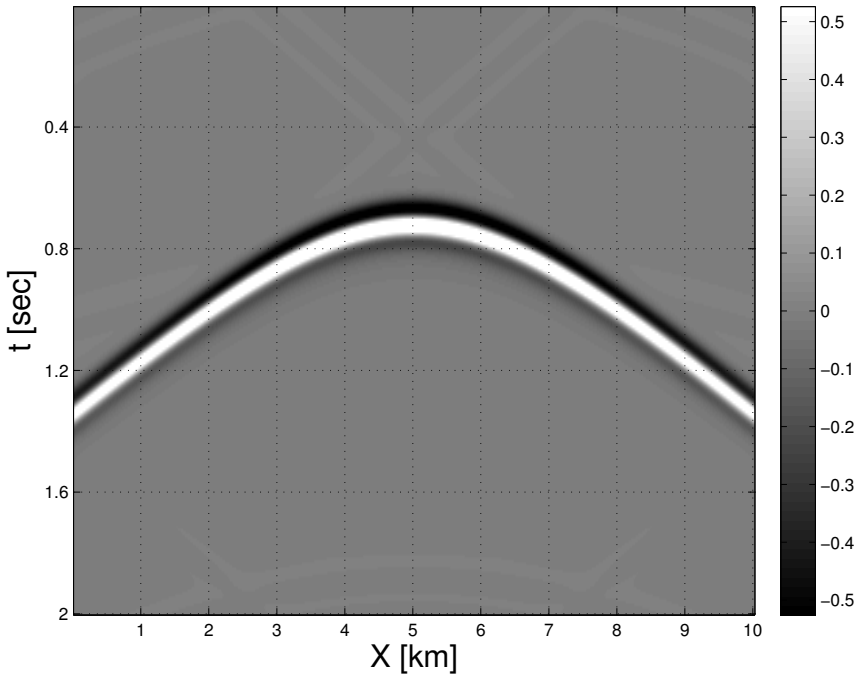

Figure 11: Background wave field at receiver depth $z = 2.5$ km for a constant homogenous velocity medium $c(\mathbf{x}) = 5$ km/s, formed by inverse Fourier transforming the frequency domain solutions of the Helmholtz equation. [**CR**]

Next for the extended linearized Born modeling, we use an extended velocity model

of the following form

$$\delta c_e(\mathbf{x},t) = v(t)\frac{1}{\sqrt{2\pi\sigma^2}}\exp\left(-\frac{(x-x_1)^2+(z-z_1)^2}{2\sigma^2}\right), \tag{16}$$

where we have chosen a product representation for the extended model with the time signature given by $v(t)$, and is modulated in space by a Gaussian centered at $(x_1 = 5 \text{ km}, z_1 = 3.5 \text{ km})$ with standard deviation $\sigma = 0.1$ km, as shown in Figure 12. We try three different cases for $v(t)$ — (a) $v(t) = \delta_0(t)$, (b) $v(t) = \delta_a(t)$ and (c) $v(t) = \delta_{-a}(t)$, where $a = 0.5$ s.

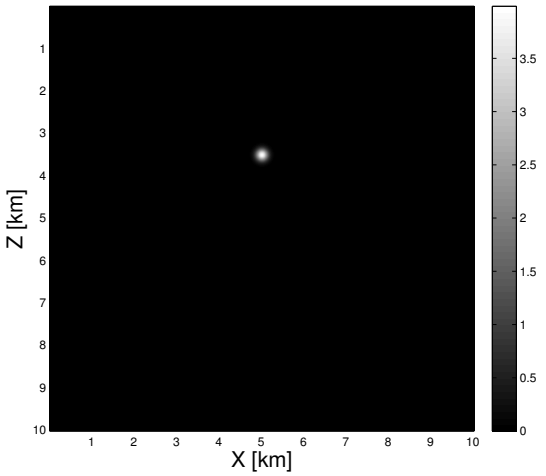

(a)

Figure 12: Spatially varying Gaussian field component of the extended velocity model $\delta c_e(\mathbf{x},t)$. [**CR**]

To use the Helmholtz solver, we proceed by discrete Fourier transforming $\delta c_e(\mathbf{x},t)$ to get $\delta\hat{c}_e(\mathbf{x},\omega)$ for each case, and at the same set of discrete angular frequencies as in the case of the background wave field. Then the forcing term in equation 12 is easily calculated as a point-wise multiplication with the already solved background wave field to get $\frac{2\omega^2}{c^3(\mathbf{x})}\hat{u}(\mathbf{x},\omega)\delta\hat{c}_e(\mathbf{x},\omega)$ at each angular frequency to be solved for. Finally, we inverse discrete Fourier transform the solutions to the Helmholtz equation to get the time domain solution. These results are again displayed for all receivers at depth $z = 2.5$ km in Figures 13, 14 and 15 for the three cases with $v(t)$ given by $\delta_0(t)$, $\delta_a(t)$ and $\delta_{-a}(t)$ respectively.

The first case with $v(t) = \delta_0(t)$ corresponds to standard Born modeled wave field, while the second case with $v(t) = \delta_a(t)$ and the third case with $v(t) = \delta_{-a}(t)$ correspond to the cases where the Born modeled wave field is delayed by +0.5s and -0.5s, respectively.

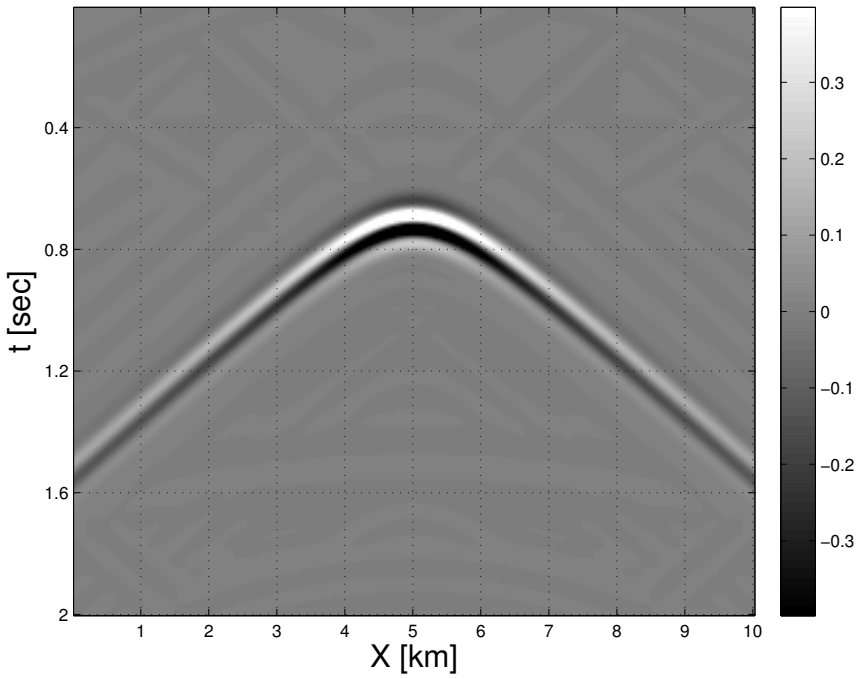

Figure 13: Extended linearized Born modeled wave field for the TFWI experiment recorded at receiver depth $z = 2.5$ km for $v(t) = \delta_0(t)$. [**CR**]

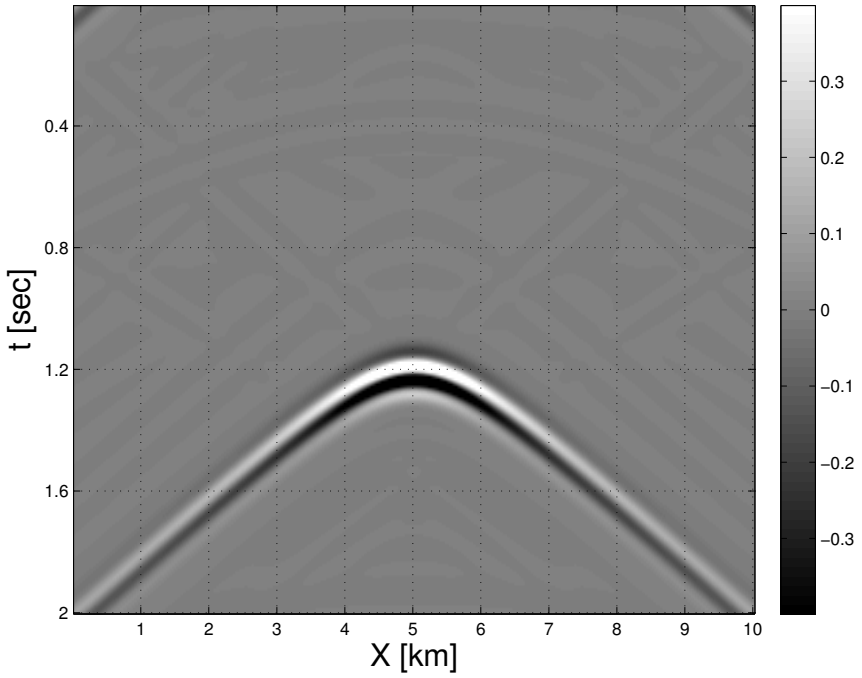

Figure 14: Extended linearized Born modeled wave field for the TFWI experiment recorded at receiver depth $z = 2.5$ km for $v(t) = \delta_a(t)$, where $a = 0.5$ s. [**CR**]

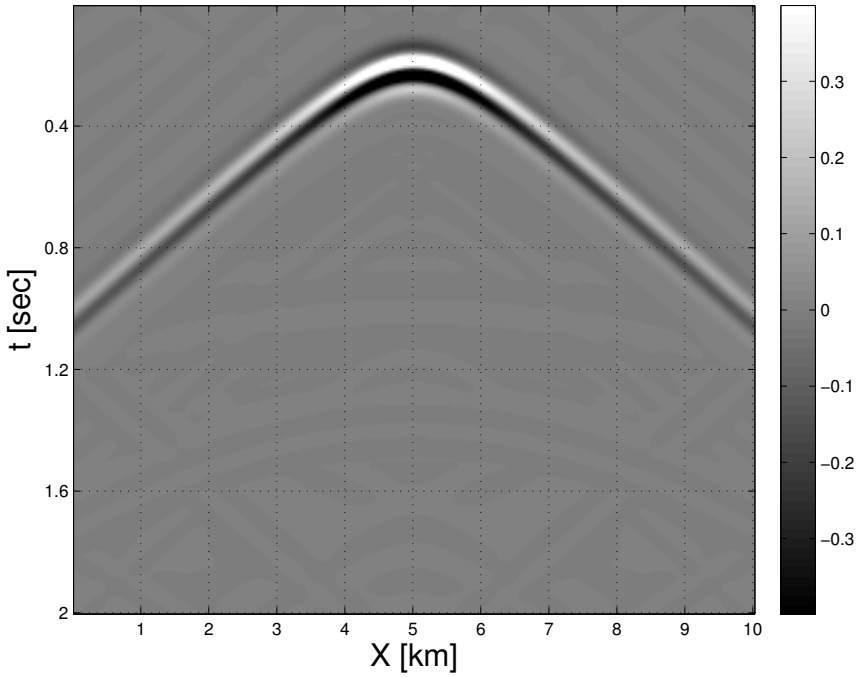

Figure 15: Extended linearized Born modeled wave field for the TFWI experiment recorded at receiver depth $z = 2.5$ km for $v(t) = \delta_{-a}(t)$, where $a = 0.5$ s. [**CR**]

DISCUSSION AND FUTURE WORK

In this paper, we have developed a 2D Helmholtz equation solver library in C++. We provided some numerical examples by solving the Helmholtz equation using the library for homogenous and inhomogenous media, for different frequencies. We also performed a Born linearization test to verify the theoretical prediction that the error is indeed quadratic with respect to the magnitude of the velocity perturbation. Finally, we showed how extended linearized Born forward modeling can be performed in the frequency domain.

Future work with this library is aimed at extending it to solve the 3D Helmholtz equation. The eventual goal of this research project, started this summer, is to use the library to solve TFWI problem in the frequency domain which will likely bring enormous computational savings. The immediate near term goal is to integrate the Helmholtz solver with an inversion library and experiment with 2D TFWI.

ACKNOWLEDGEMENT

We would like to thank Prof. Lexing Ying and Prof. Andras Vasy for helpful discussions on the numerical and analytical aspects of the Helmholtz equation. We would also like to thank Prof. Stew Levin and Eileen Martin for proof-reading and suggesting valuable edits that greatly improved the quality of this paper.

REFERENCES

Biondi, B. and A. Almomin, 2014, Simultaneous inversion of full data bandwidth by tomographic full waveform inversion: Geophysics, **79**, no. 3, WA129–WA140.

Davis, T. A., 2004, Algorithm 832: Umfpack v4. 3—An unsymmetric-pattern multifrontal method: ACM Transactions on Mathematical Software (TOMS), **30**, 196–199.

———, 2006, Direct methods for sparse linear systems: SIAM.

Johnson, S. G., 2008, Notes on perfectly matched layers (PMLs): Lecture notes, Massachusetts Institute of Technology, Massachusetts, **29**.

Liu, F. and L. Ying, 2016, Additive sweeping preconditioner for the Helmholtz equation: Multiscale Modeling & Simulation, **14**, 799–822.

Sommerfeld, A., 1949, Partial differential equations in physics, volume **1**: Academic Press.